Revealing the Impact of Ferromagnetic Elements on Fe-Based Amorphous Alloy Properties via *ab initio* molecular dynamics simulations and Experiments*

Jin-Hua Xiao(肖晋桦)[1], Da-Wei Ding(丁大伟)[2**], Lin Li(李琳)[1], Yi-Tao Sun(孙奕韬)[2], Mao-Zhi Li(李茂枝)[3], Wei-Hua Wang(汪卫华)[2]

[1]State Key Laboratory of Alternate Electrical Power System with Renewable Energy Sources, North China Electric Power University, Beijing 102206, China
[2] Institute of Physics, Chinese Academy of Sciences, Beijing 100190, China
[3]Department of Physics and Beijing Key Laboratory of Opto-electronic Functional Materials & Micro-nano Devices, Renmin University of China, Beijing 100872, China

*Supported by the National Natural Science Foundation of China under Grant No. 10225417 and the National Basic Research Program of China under Grant No. 2006CB601003.
**Corresponding author. Email: dingdawei@iphy.ac.cn

High saturation magnetic flux density (B_s) is essential for the development of Fe-based amorphous alloys in electromagnetic devices and motors. However, achieving high B_s often compromises the glass-forming ability (GFA) of Fe-based amorphous alloys. This study investigates the effects of ferromagnetic elements (Fe, Co, and Ni) on the microstructure and magnetic properties of $Fe_{86}B_7C_7$ amorphous alloys through both experiments and *ab initio* molecular dynamics simulations. By analyzing both experimental and simulation results, the relationship is explored between atomic structures, GFA, and magnetic properties of these amorphous alloys. The research indicates that the GFA of the alloys is correlated with the proportion of icosahedral clusters and body-centered cubic clusters. The addition of Co and Ni not only improves the GFA of alloys, but also effectively increases the overall magnetic moment with an appropriate amount of Co and a minor amount of Ni. This increase in magnetic moment primarily arises from the enhancement of the magnetic moment of Fe atoms, resulting from the redistribution between the spin-up and spin-down electrons of Fe-3d orbits, as well as the strong exchange interactions between Fe-Co and Fe-Ni pairs. The results obtained offer valuable insights into the correlation between atomic structure and magnetic properties in these amorphous alloys, and suggest potential directions for the optimization of Fe-based amorphous alloys.

PACS: 61.43.Dq, 81.05.Kf, 71.15.Pd, 75.50.Kj

Amorphous alloys, as a novel soft magnetic material, have extensive applications in electromagnetic equipment and motors due to their exceptional magnetic properties.[1-5] In comparison with conventional silicon steel, Fe-based amorphous alloys exhibit significant advantages in terms of core loss and energy conversion efficiency, making them promising alternatives for core materials in distribution transformers.[6] However, the saturation flux density (B_s) of amorphous alloys is still lower than that of silicon steel (approximately 2.0 T), e.g., the commercial amorphous alloy (METGLAS 2605SA1) only achieves a B_s of 1.56 T.[7] Recent research has shown microalloyed and optimized the production process can continuously enhance the magnetic properties of Fe-based amorphous alloys.[8] However, the improvement of magnetic properties often comes at the expense of reduced glass-forming ability (GFA).[9-11] Consequently, the trade-off between B_s and GFA in Fe-based amorphous alloys remains a major challenge.[12-14]

Previous studies have demonstrated that the addition of appropriate Co into Fe-based

amorphous alloys can effectively enhance the B_s.[15,16] For instance, Inoue et al. successfully synthesized an alloy with the B_s as high as 1.92 T and the H_c of only 2 A/m by incorporating Co into high-Fe content amorphous alloys.[17] Additionally, some researches have indicated that the addition of Ni into Fe-based amorphous alloys can enhance the GFA and mechanical properties of the alloy.[18] However, the addition of Ni may lead to a reduction in B_s and adversely affect the magnetic properties of the alloy.[19] Although these experimental researches optimize the properties of Fe-based amorphous alloys, the theoretical basis of the microstructural changes in these alloys caused by the doping of ferromagnetic elements remains unclear. In recent years, *ab initio* molecular dynamics (AIMD) simulations have provided valuable insights into the microstructure in the amorphous alloys.[20-23] AIMD simulations have revealed that the doping of Co and Ni can enhance the exchange splitting energy, thereby increase the magnetic moment of Fe atoms.[24,25] Researches combining AIMD simulations with experimental results might further promote the advancement of materials design of amorphous soft magnetic material.[26] Specifically, whether Ni doping can enhance the B_s of Fe-based amorphous alloys worth systematic investigation. Therefore, it is crucial to systematically investigate the effects of ferromagnetic elements on atomic structure and magnetism in Fe-based amorphous alloys, particularly when Co and Ni are co-doped.

This study investigates the effects of ferromagnetic elements (Fe, Co, and Ni) on the atomic structures and magnetic properties of $Fe_{86}B_7C_7$-based amorphous alloys through experimental methods and AIMD simulations. The results elucidate the mechanisms by which Co and Ni enhance the GFA of the alloy from an atomic structural perspective. Furthermore, minor Ni doping is shown to effectively increase the magnetic moment of Fe atoms, with this finding validated through experiments. Thus, a theoretical foundation is established for the development of Fe-based amorphous alloys, supporting the design of alloys with both excellent GFA and high magnetic saturation.

Experimental and Simulation Methods. Alloys ingots with nominal compositions of $Fe_{86-x}Co_xB_7C_7$ (x=0-10 at.%; denoted as Co_x)、$Fe_{86-y}Ni_yB_7C_7$ (y=0-10 at.%; denoted as Ni_y) and $Fe_{86-x-y}Co_XNi_yB_7C_7$ (x= 5, y=3; x=10, y= 3 and 5 at.%; denoted as Co_xNi_y) were prepared by induction melting mixtures of pure Fe, Co, Ni metals, and pre-alloys of Fe-B, Fe-C in an argon atmosphere. The as-spun ribbons were then fabricated using the single roller melt-spinning method with a linear velocity of 40 m/s in an argon atmosphere. These ribbons have a thickness of approximately 20 μm and a width of about 1 mm. The structure of the as-spun ribbons was characterized using X-ray diffraction (XRD DX-2700BH) with a Cu Kα source. The thermodynamic parameters of all amorphous alloys were determined using differential scanning calorimetry (DSC 8000) and simultaneous thermal analyzer (STA 8000) under an argon flow at a heating rate of 10 K/min. Magnetization of the as-spun ribbons were measured at room temperature using a vibrating sample magnetometer (VSM) with a maximum applied field of 800 kA/m. AIMD simulations based on density functional theory (DFT) are performed using the Vienna *ab initio* simulation package (VASP).[27] The projected augmented wave (PAW) method is used to accurately describe the electron-ion interactions, and the generalized gradient approximation (GGA) is employed to effectively capture the exchange correlation among electrons.[28] Simulations are conducted in the canonical ensemble (NVT), with temperature control provided by a Nosé-Hoover thermostat. A cubic supercell containing 200 atoms with periodic boundary conditions is generated by the Monte Carlo method, and the supercell size is determined by the alloy density at room temperature. Brillouin zone sampling is performed at the Γ point. Alloys are equilibrated for 1500 steps (2 fs for each step) at 1800 K to remove the memory from the initial configurations, then cooled to 1200 K and 300 K at a rate of 2×10^{14} K/s. For accurate electron density of states (DOS) calculation, a 3×3×3 k-points mesh is adopted. The DOS is calculated with consideration of spin polarization, and an analysis of the DOS is used to discuss the magnetic moments of the alloys.

Results and discussion The XRD patterns of the as-spun ribbons $Fe_{86-x-y}Co_xNi_yB_7C_7$ (x=0-10; y=0-10 at. %) are presented in Figure S1. All samples exhibit broad diffraction peaks around $2\theta \approx 45°$, with no distinct crystallization peaks observed, indicating that all ribbons have a fully amorphous structure. Figure 1 illustrates the DSC curves of these amorphous alloys. For the $Fe_{86}B_7C_7$ amorphous alloy, the DSC curve does not exhibit a distinct glass transition temperature

(T_g) but displays a clear Curie temperature (T_c). Upon the addition of Co or Ni, the DSC curve shows a noticeable T_g. However, no T_c is observed in the DSC curves of the other alloys, potentially due to the addition of Co and Ni enhancing the T_c of the alloy, resulting in T_c approaching or exceeding T_{x1}. Based on the Bethe-Slater curve, it is observed that the atomic exchange interaction between Fe-Co and Fe-Ni pairs is stronger than that between Fe-Fe pairs. Consequently, the addition of Co or Ni leads to the replacement of some Fe-Fe pairs with Fe-Co or Fe-Ni pairs, thereby enhancing the average atomic exchange interaction among magnetic atoms and increasing the T_c of the alloy. Table 1 summarizes the thermodynamic parameters of all amorphous alloys. Notably, T_g and T_{x1} initially increase with increasing Co content, but then decrease. The addition of Ni significantly enhances both T_g and T_{x1}, especially in the case of the Ni_{10} alloy where they reach their maximum values. Moreover, co-doping with Co and Ni has a relatively minor effect on the T_g and T_{x1} of the alloy. To further evaluate the GFA of the alloys, the thermodynamic parameters ΔT (T_{x1}-T_g) and T_{rg} (T_g/T_l) are analyzed, as shown in Table 1. The results show that the addition of Co and Ni leads to an increase in ΔT and T_{rg}, with Ni exerting a more pronounced influence on these parameters. This indicates the addition of either Co or Ni enhances the GFA of the alloy, with the improvement being particularly pronounced for Ni. Among all amorphous alloys, the Ni_{10} alloy is expected to exhibit the best GFA. To verify this conclusion, the critical thicknesses of $Fe_{86}B_7C_7$, Co_{10}, Ni_{10}, and Co_5Ni_3 alloys are measured by controlling the roll speed during the preparation process. The critical thicknesses are found to be 23 μm, 32 μm, 45 μm, and 33 μm, respectively. This further demonstrates that the substitution of Fe with Co and Ni significantly enhances the GFA of the $Fe_{86}B_7C_7$ alloy.

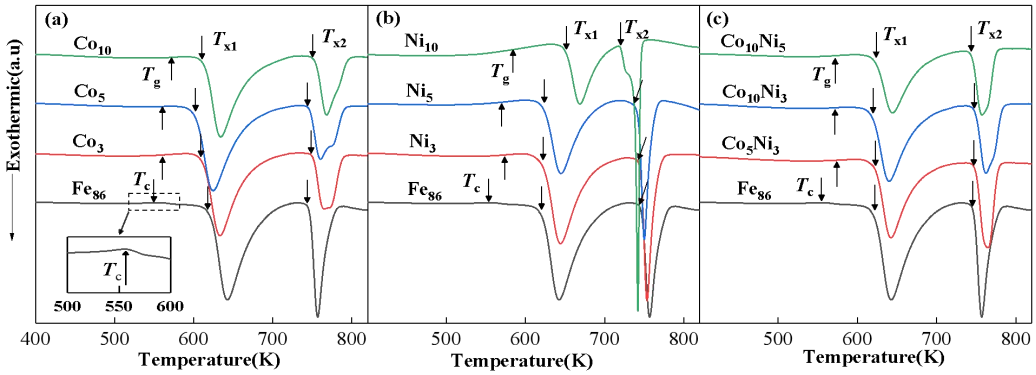

Fig. 1. DSC curves of all amorphous alloys: (a) $Fe_{86-x}Co_xB_7C_7$(x=0-10 at. %), (b) $Fe_{86-x}Ni_xB_7C_7$(x=0-10 at. %), (c) $Fe_{86-x-y}Co_XNi_yB_7C_7$(x= 5, y=3; x=10, y= 3 and 5 at. %).

Table 1. The thermodynamic parameters of all amorphous alloy (T_g is the glass transition temperature, T_{x1} is the first crystallization temperature, T_{x2} is the second crystallization temperature, T_l is the melting temperature, $\Delta T = T_{x1}$-T_g, and $T_{rg} = T_g/T_l$).

Amorphous alloys	T_g (K)	T_{x1} (K)	T_{x2} (K)	T_l (K)	ΔT(K)	T_{rg}
$Fe_{86}B_7C_7$	—	621	743	1458	—	—
$Fe_{83}Co_3B_7C_7$	563	606	750	1394	43	0.404
$Fe_{81}Co_5B_7C_7$	561	603	745	1388	42	0.405
$Fe_{76}Co_{10}B_7C_7$	571	615	751	1374	44	0.416
$Fe_{83}Ni_3B_7C_7$	572	623	742	1392	51	0.411
$Fe_{81}Ni_5B_7C_7$	570	625	737	1389	57	0.410
$Fe_{76}Ni_{10}B_7C_7$	582	653	721	1368	71	0.425
$Fe_{78}Co_5Ni_3B_7C_7$	574	624	747	1386	50	0.414
$Fe_{73}Co_{10}Ni_3B_7C_7$	567	620	746	1382	53	0.410
$Fe_{71}Co_{10}Ni_5B_7C_7$	573	624	744	1376	51	0.416

To investigate the influence of Co and Ni on the GFA of the alloys from an atomic structural perspective, various structural parameters are calculated, including the pair distribution function (PDF), Voronoi polyhedron (VP), and bond pairs. The commonly used form of the PDF is the Faber-Ziman form, expressed as follows:[29]

$$g_{\alpha\beta}(r) = \frac{N}{4\pi^2 \rho N_\alpha N_\beta} \sum_{i=1}^{N_\alpha} \sum_{j=1}^{N_\beta} \delta\left(r - r_{ij}\right) \quad , \tag{1}$$

where N is the total number of atoms, N_α and N_β are the numbers of atoms of type α and type β, ρ is the atomic density, and r_{ij} is the distance between atoms i and j. Figure 2 presents the PDF curves of all alloys simulated at 1800 K and 300 K. As temperature decreases, the height of the first peak increases, indicating enhanced short-range order. Simultaneously, the splitting of the second peak suggests the emergence of mid-range order, providing evidence for the formation of amorphous structures during AIMD simulations.[30] This splitting is typically attributed to the uneven connectivity within atomic clusters.[21] The transition from liquid to glassy state of the alloy is likely associated with a combination of increased local topological order and cluster connectivity formation, giving rise to the characteristic PDF curve.[31] Additionally, at 300 K, a minor sub-peak appears on the left shoulder of the first peak in the PDF curves for all alloys. This sub-peak does not indicate crystallization but rather reflects the inconsistent positions of the first peak values for $g_{\text{Fe-Fe}}(r)$, $g_{\text{Fe-B}}(r)$, and $g_{\text{Fe-C}}(r)$.

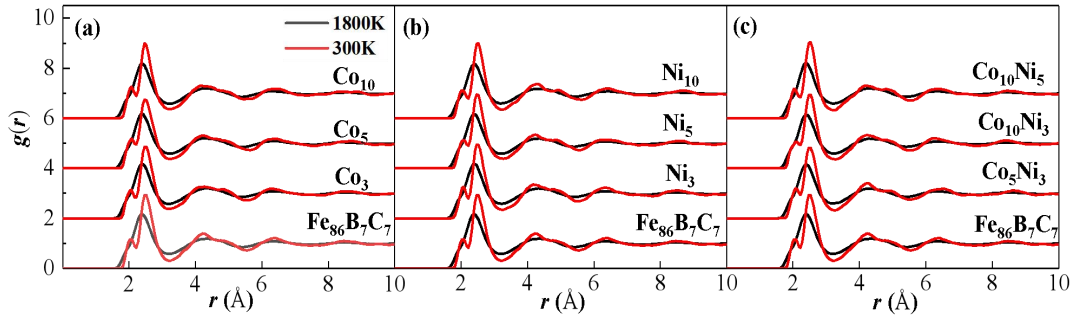

Fig. 2. Total PDFs of all alloys at 1800 K and 300 K: (a) $Fe_{86-x}Co_xB_7C_7$(x=0-10 at. %), (b) $Fe_{86-x}Ni_xB_7C_7$(x=0-10 at. %), (c) $Fe_{86-x-y}Co_XNi_yB_7C_7$(x= 5, y=3; x=10, y= 3 and 5 at. %).

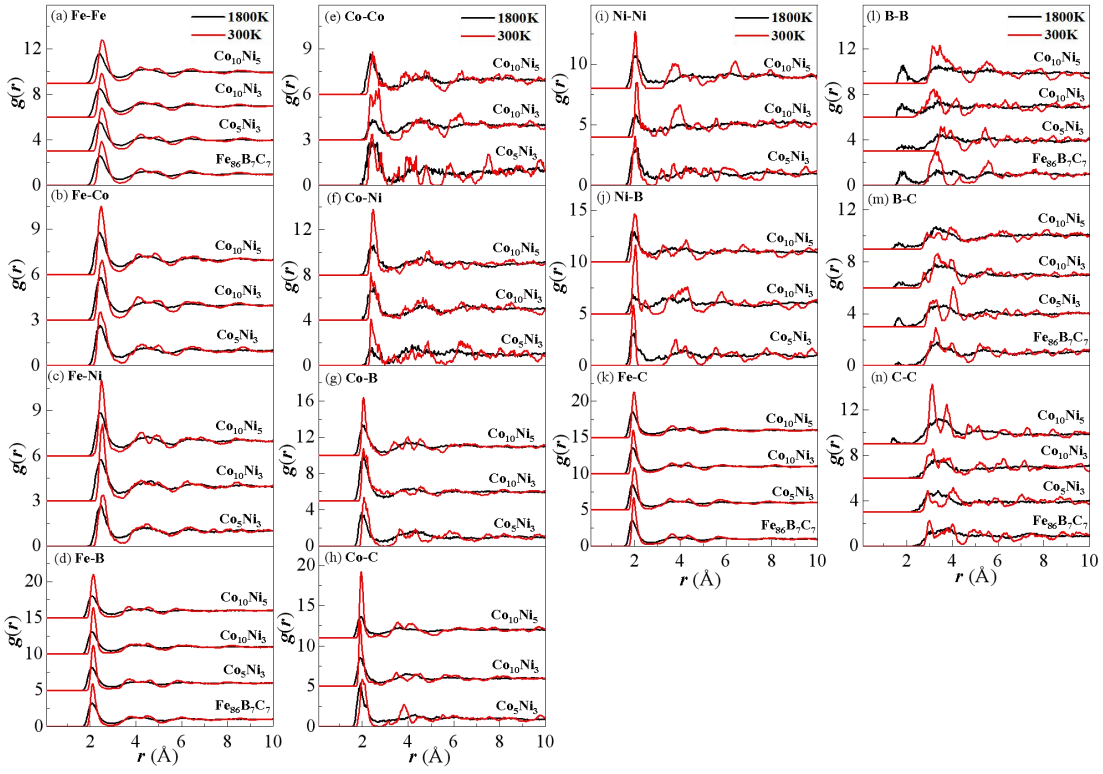

Fig. 3. PPDFs of $Fe_{86-x-y}Co_XNi_yB_7C_7$(x= 5, y=3; x=10, y= 3 and 5 at. %) alloys at 1800K and 300 K.

Figure 3 displays the partial pair distribution function (PPDF) curves for $Fe_{86-x-y}Co_XNi_yB_7C_7$(x= 5, y=3; x=10, y= 3 and 5 at. %) alloys at 1800 K and 300 K. Due to the similarity of the PPDF curves of other alloys, we present them in Figure S2 and S3. The results indicate that the PPDF curves for Fe, Co, and Ni atoms are similar to the PDF curves of the alloys, with a higher first peak at 300 K and a splitting of the second peak. The position of the first peak in the PPDF curve for Fe atoms shifts significantly to the right with increasing temperature, indicating changes in bond length. This shift is attributed to the differences in bond lengths between Fe atoms in ferromagnetic and paramagnetic states; specifically, the bond length of Fe atoms is greater in the ferromagnetic state compared to the paramagnetic state, resulting in a corresponding shift in the position of the overall PDF curve's first peak. Additionally, the first peak in the PPDF curves for B and C atoms is less pronounced, suggesting better solute-solute avoidance.[32] This facilitates the formation of stable atomic clusters, which stabilizes the alloy in its molten and amorphous states, reduces compositional segregation, and ultimately improves the GFA of the alloy.

The bond lengths between pairs of Fe, Co, and Ni atoms can be inferred from the positions of the first peaks in the PPDF curves, as summarized in Table S1. To confirm whether chemical bonds are formed between these atoms, we compare the positions of the first peaks with their atomic radii and the sum of their radii (r_{sum}). The results show that the positions of the first peaks are consistently smaller than the corresponding sums of atomic radii, suggesting the presence of covalent bonding between Fe, Co, and Ni atoms, as well as between these atoms and B and C atoms. According to the Bethe-Slater curve, the bond length of Fe atoms affects their magnetic moment, with longer bond lengths generally corresponding to larger atomic magnetic moments within a certain range.[16] The addition of Co or Ni into the $Fe_{86}B_7C_7$ amorphous alloy results in increased bond lengths of Fe atoms, indicating an enhancement in the magnetic moment of Fe atoms. Among all alloys, the $Co_{10}Ni_5$ alloy is expected to exhibit the largest Fe atomic magnetic moment, providing an advantage for the magnetic properties of the alloys.

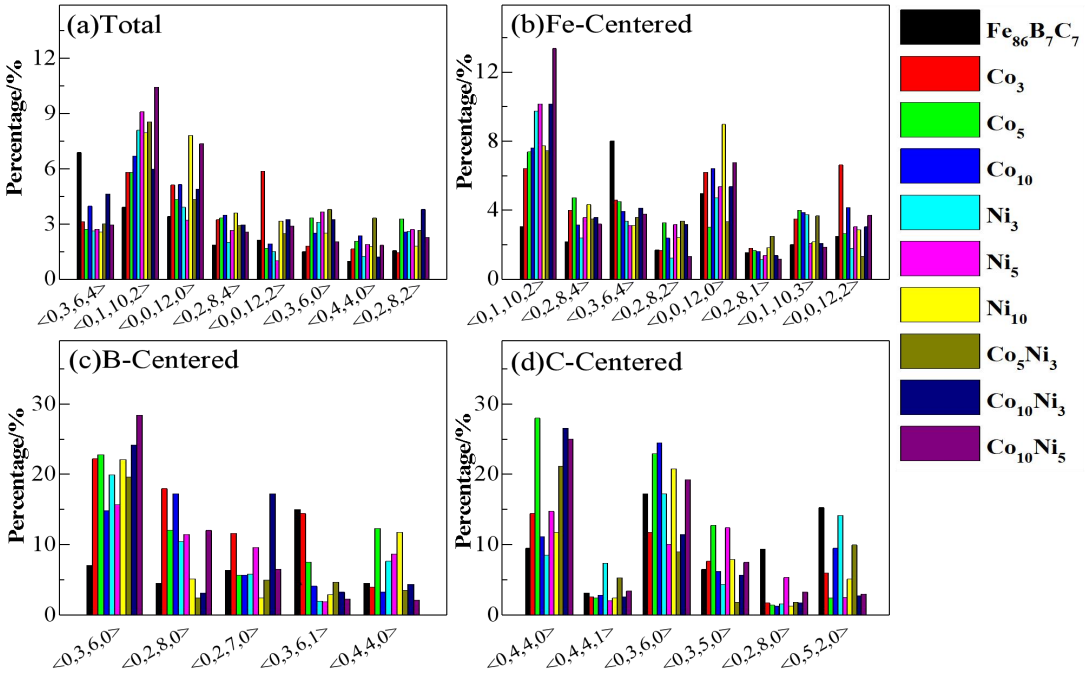

Fig. 4. Distribution of atomically centered VP polyhedra in all amorphous alloys: (a) Total; (b) Fe-centered; (c) B-centered; (C) C-centered.

To further elucidate the local atomic structures of the amorphous alloys, we analyze the major VPs for all amorphous alloys at 300 K, as shown in Figure 4 and Figure 5. The VP index is defined as $<n_3, n_4, n_5, n_6>$, where n_i represents the number of i-edged faces in the Voronoi polyhedron, and the sum of n_i gives the coordination number (CN) of the atom.[33] The analysis

reveals that the Fe-centered polyhedra predominantly consist of <0,1,10,2>, <0,0,12,0>, <0,2,8,4>, <0,3,6,4>, and <0,2,8,2>. The polyhedra <0,0,12,0> correspond to perfect icosahedral structures, while <0,1,10,2> represents icosahedral-like structures, and <0,3,6,4> indicates a deformed body-centered cubic (bcc) structure, revealing a predominance of icosahedral-like and bcc clusters around Fe atoms. The B-centered polyhedra mainly include <0,3,6,0> and <0,3,6,1>, which correspond to tricapped trigonal prism (TTP) structures and distorted TTP structures, respectively, as well as <0,2,8,0> and <0,4,4,0>, representing Archimedean anti-prismatic structures. For C-centered polyhedra, in addition to a high frequency of <0,4,4,0> and <0,3,6,0> structures, various distorted TTP structures such as <0,3,5,0> and <0,5,2,0> are present. This indicates that the local structures around the B and C atoms in all amorphous alloys are predominantly trigonal prismatic in nature.

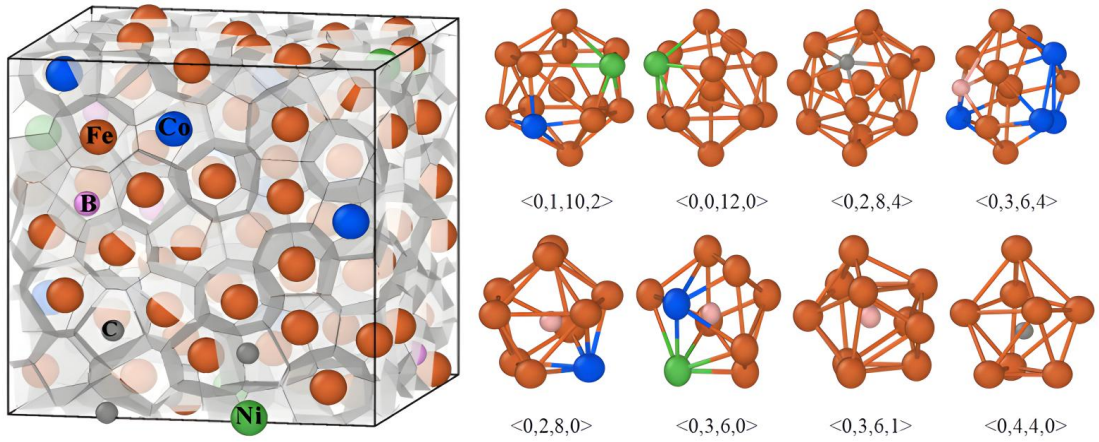

Fig. 5. The model of typical VPs in all amorphous alloys.

In general, due to their five-fold symmetry, icosahedral structures tend to form dense atomic packing, thereby inhibits periodic ordering and suppresses the nucleation of crystalline phases.[30] Consequently, amorphous alloys with strong GFA typically exhibit a high content of icosahedral structures, as reflected in the coordination number distributions. Figure 6 illustrates the coordination number distribution of Fe atoms within all amorphous alloys at 300 K, along with their average coordination numbers. Comparative results indicate that the average coordination number of Fe atoms decreases with the addition of Co or Ni, suggesting the formation of more icosahedral clusters around the Fe atoms within the alloy. Such cluster structures are generally more stable and enhance the GFA of amorphous alloys.

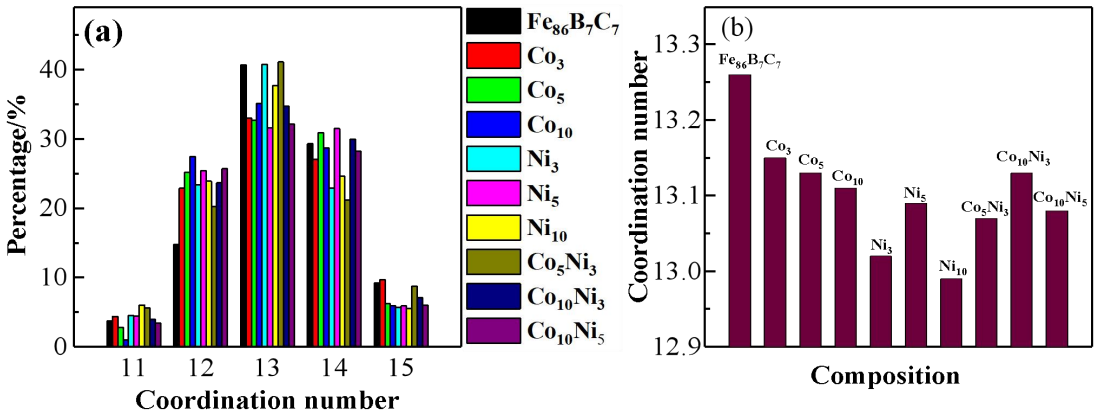

Fig. 6. (a) Distributions of coordination number in Fe-centered clusters for all amorphous alloys; (b) The average coordination number of Fe atoms in all amorphous alloys at 300 K.

The atomic structural configurations of the alloys are further analyzed through the HA bond pair index method. The HA bond pair index utilizes four indices *i*, *j*, *k*, and *l* to describe bonding interactions between pairs of atoms and their shared neighboring atoms.[34] According to the

nearest neighbor of $g_{ij}(r)$, if the atom *A* and *B* form a bond, $i = 1$; otherwise, $i = 2$; j represents the number of neighboring atoms that form bonds with both the *A* atom and *B* atom; k denotes the number of bonds formed by these common neighbors; l is a special classifying index. The bond pair distributions of all alloys are shown in Figure 7. The four compositions of the amorphous alloys predominantly consist of 1541, 1551, 1431, 1441, and 1661 bond pairs. According to the HA index method, 1541, 1551, and 1431 bond pairs are associated with icosahedral structures while 1441 and 1661 bond pairs correspond to bcc structures. The analysis reveals that the microstructure of all amorphous alloys is primarily composed of icosahedral and bcc structures, with a significantly higher proportion of bond pairs associated with icosahedral structures compared to those associated with bcc structures.

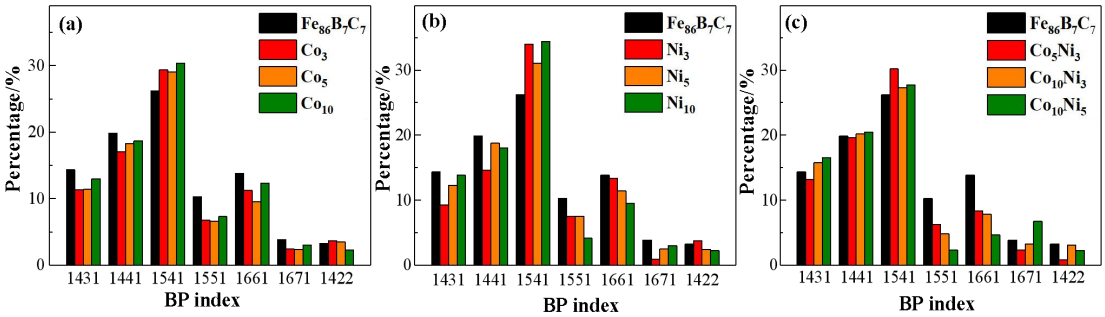

Fig. 7. Bond pairs distribution of all alloys at 300 K: (a) $Fe_{86-x}Co_xB_7C_7$(x=0-10 at. %), (b) $Fe_{86-x}Ni_xB_7C_7$(x=0-10 at. %), (c) $Fe_{86-x-y}Co_XNi_yB_7C_7$(x= 5, y=3; x=10, y= 3 and 5 at. %).

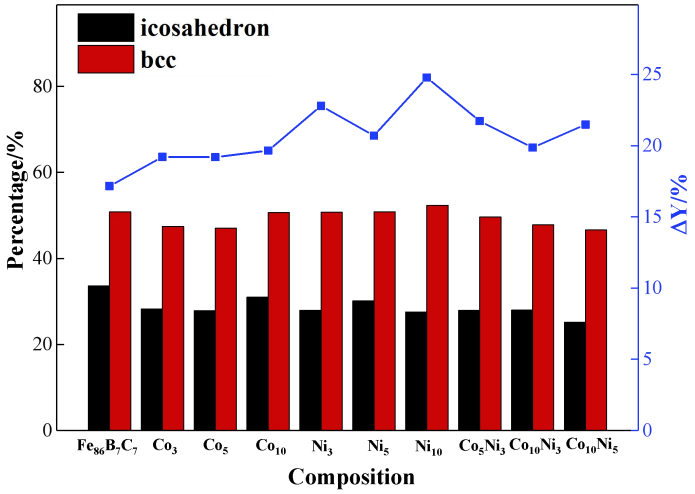

Fig. 8. Ratios of icosahedral and bcc polyhedra in all amorphous alloys at 300 K and their differences.

As previously discussed, a high content of icosahedral structures and a low content of bcc structures are beneficial for enhancing the GFA of the alloys. To further investigate this, the ratios and discrepancies between bond pairs corresponding to icosahedral and bcc structures at 300 K are statistically analyzed, as illustrated in Figure 8. The results indicate that the addition of Co or Ni significantly increases the difference between the contents of bond pairs corresponding to icosahedral and bcc structures, with the Ni_{10} composition showing the largest difference. This finding is consistent with prior experimental results, suggesting that the Ni_{10} alloy possesses optimal GFA. Moreover, it highlights the close relationship between good GFA in this series of alloys and maintaining a high content of icosahedral structures coupled with a low content of bcc structures.

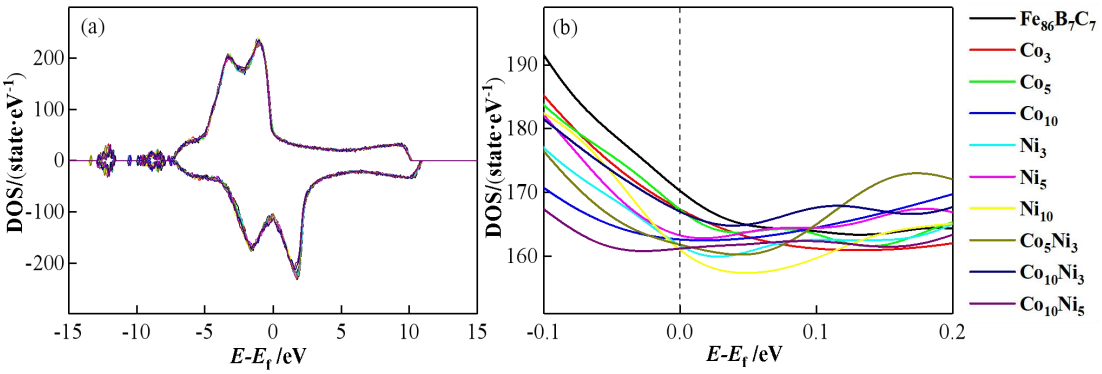

Fig. 9. (a) The total DOS of all amorphous alloys; (b) The sum of electron state densities in the spin up and spin down orbits near Fermi levels of all amorphous alloys.

To investigate the effects of Co and Ni doping on the magnetic properties of the $Fe_{86}B_7C_7$ amorphous alloy, we conducted a detailed analysis of its electronic density of states (DOS) and magnetic moments. Figure 9 (a) illustrates the total DOS of the $Fe_{86-x-y}Co_xNi_yB_7C_7$ (x=0-10; y=0-10 at. %) amorphous alloys, revealing that the total DOS is generally similar across all compositions, exhibiting a characteristic asymmetrical splitting of the spin-up and spin-down bands. This band splitting leads to different magnetic moments for the spin-up and spin-down electrons, and when the Fermi level falls within the gap of the spin-down band (referred to as the pseudogap), pronounced ferromagnetism is observed in the amorphous alloy.[34] Previous research has indicated that a higher DOS near the Fermi level is associated with an increased number of non-bonding pairs in the system.[24,31] This phenomenon can weaken interatomic interactions and diminish the stability of the local atomic structure. As depicted in Figure 9 (b), the DOS values for all amorphous alloys suggest that the $Fe_{86}B_7C_7$ alloy has the highest DOS value. In contrast, the DOS values for Co_3, Co_5, and $Co_{10}Ni_5$ alloys are slightly lower than that of $Fe_{86}B_7C_7$, while the other compositions exhibit the lowest DOS values. These findings imply that the interatomic bonding in the Co_{10}, Ni_3, Ni_5, Ni_{10}, Co_5Ni_3, and $Co_{10}Ni_5$ amorphous alloys is stronger, facilitating the formation of a stable amorphous structure and enhances the GFA.

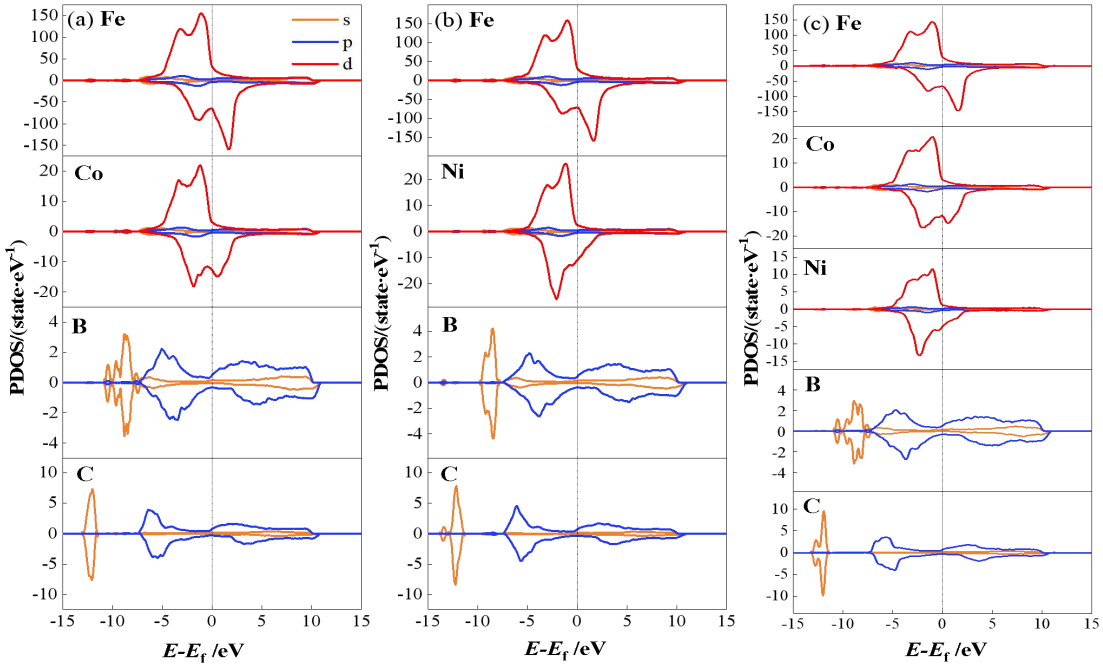

Fig. 10. The PDOS of three amorphous alloys: (a) $Fe_7Co_{10}B_7C_7$, (b) $Fe_{76}Ni_{10}B_7C_7$, (c) $Fe_{71}Co_{10}Ni_5B_7C_7$.

Given the similarity in the DOS among Fe, Co, Ni, B, and C in all amorphous alloys, we selected the DOS of $Fe_{76}Co_{10}B_7C_7$, $Fe_{76}Ni_{10}B_7C_7$, and $Fe_{71}Co_{10}Ni_5B_7C_7$ for further analysis, as shown in Figure 10. The analysis reveals that the total DOS of these alloys is predominantly

derived from the Fe-3d orbital electron states, with contributions from Co-3d and Ni-3d orbitals being relatively minor. These orbitals are the primary contributors to the alloy's magnetic properties. Additionally, hybridization between the Fe-3d, Co-3d, Ni-3d, and B-2p, C-2p orbitals is observed. This interatomic orbital hybridization can modify the exchange energy or the energy gap between orbitals, thereby facilitating the formation of bonds between atoms.[33] This finding suggests the existence of chemical bonds between these magnetic atoms and the B and C atoms, enhancing structural stability and playing a critical role in glass formation.

From the Figure 10, it is also observed that the DOS of Co is similar to that of Fe, exhibiting a significant pseudogap, indicating that Co demonstrates a certain degree of ferromagnetism with its atomic magnetic moment likely exceeding that of Ni. To further investigate the impact of these three magnetic elements on the alloy's magnetism, we summarized the average atomic magnetic moments of all the amorphous alloys at 300 K, as presented in Table 2. It is apparent that the average magnetic moment of Fe atoms in all alloys exceeds 2 μ_B, primarily contributed by the Fe-3d orbital magnetic moment. Meanwhile, both Co and Ni exhibit certain magnetic moments with average atomic values approximately being 1.5 μ_B and 0.5 μ_B, respectively. The contributions from B and C to the system's magnetic moment are minimal, with average values of approximately -0.15 μ_B and -0.13 μ_B, respectively. Comparisons reveal that the average magnetic moment of Fe increases with the addition of Co and Ni. And both Co and Ni doping significantly enhance the magnetic moment of Fe atoms, with Co having a more pronounced effect than Ni. Moreover, the simultaneous introduction of Co and Ni further enhances the Fe magnetic moment, reaching up to 2.3 μ_B. There are two factors contributing to the enhancement of the magnetic moment of Fe atoms. Firstly, upon the addition of Co and Ni, there is a redistribution of the Fe-3d electrons between spin-up and spin-down states in response to changes in the number and type of nearest neighbors surrounding the Fe atoms,[25] as depicted in Figure 6. Secondly, the exchange interactions between Fe-Co and Fe-Ni pairs are stronger than those between Fe-Fe pairs, resulting in an increase in T_c and enhancing both the ferromagnetic properties of the alloy and the magnetic moment of the Fe atoms.[16]

Table 2. The calculated average total magnetic moments $M_{cal\text{-}total}$ (μ_B/atom) compared with the experimental value $M_{exp\text{-}total}$ (μ_B/atom)and average local magnetic moments (μ_B/atom) of various elements for all amorphous alloys.

Alloys	$M_{exp\text{-}total}$	$M_{cal\text{-}total}$	$m_{cal\text{-}Fe}$	$m_{cal\text{-}Co}$	$m_{cal\text{-}Ni}$	$m_{cal\text{-}B}$	$m_{cal\text{-}C}$
$Fe_{86}B_7C_7$	1.605	1.815	2.135	—	—	-0.168	-0.137
$Fe_{83}Co_3B_7C_7$	1.623	1.839	2.195	1.336	—	-0.171	-0.146
$Fe_{81}Co_5B_7C_7$	1.653	1.853	2.226	1.404	—	-0.161	-0.138
$Fe_{76}Co_{10}B_7C_7$	1.672	1.865	2.282	1.497	—	-0.152	-0.128
$Fe_{83}Ni_3B_7C_7$	1.619	1.823	2.205	—	0.504	-0.171	-0.148
$Fe_{81}Ni_5B_7C_7$	1.596	1.808	2.225	—	0.546	-0.164	-0.141
$Fe_{76}Ni_{10}B_7C_7$	1.563	1.746	2.252	—	0.561	-0.158	-0.136
$Fe_{78}Co_5Ni_3B_7C_7$	1.675	1.845	2.275	1.521	0.484	-0.156	-0.135
$Fe_{73}Co_{10}Ni_3B_7C_7$	1.660	1.826	2.289	1.577	0.546	-0.158	-0.127
$Fe_{71}Co_{10}Ni_5B_7C_7$	1.648	1.797	2.298	1.547	0.576	-0.152	-0.127

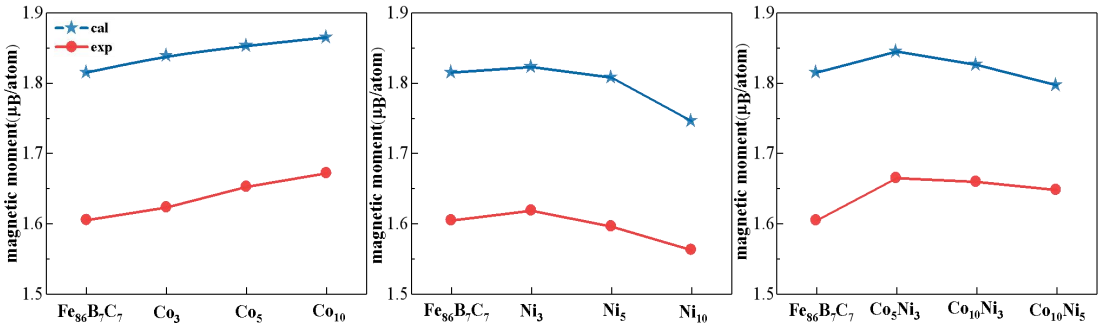

Fig. 11. Comparison of experimental and computational results of magnetic moments for all amorphous alloys.

To clarify the influence of Co and Ni on magnetism, we analyzed the total magnetic moments of all amorphous alloys, as depicted in Figure 11. The addition of Co results in a positive correlation between the total magnetic moment and Co content. In contrast, the total magnetic moment initially increases with the addition of Ni, before subsequently decreasing at higher contents. When both Co and Ni are added, the total magnetic moment reaches its maximum at the Co_5Ni_3 alloy. It can be observed that excessive addition of Co and Ni can diminish the overall magnetic moment due to diffusion effects, as this reduces the Fe content and contributes a relatively lower magnetic moment. In this study, both Co and Ni contents are maintained below 10%, since Co has a higher magnetic moment than Ni, ensuring that there is no decrease in the total magnetic moment with increasing Co content. To validate the theoretical simulation results, we measured the average atomic magnetic moments of all amorphous alloys, as shown in Figure 11. The results indicate that the trends in average atomic magnetic moments from both simulation and experimental data are generally consistent, confirming that the appropriate addition of Co and a minor addition of Ni can indeed enhance the total magnetic moment of the alloy.

In summary, the influence of ferromagnetic elements (Fe, Co, and Ni) on the microstructure and magnetic properties of Fe-based amorphous alloys has been systematically investigated. Through AIMD simulations and experimental methods, we demonstrate that the addition of Co and Ni significantly changes the local structure of the alloys. This change in local structure is characterized by an increased proportion of icosahedral structures and a decreased proportion of bcc structures, indicating enhanced structural stability, especially at a Ni content of 10%. This observation correlates with the experimentally observed improvement in GFA, highlighting the close relationship between GFA and the content of icosahedral structures. Furthermore, our simulation results demonstrate that Co and Ni doping effectively enhance the magnetic moment of Fe atoms due to the redistribution of the Fe-3d charge between spin-up and spin-down states in response to changes in the local environment surrounding the Fe atoms, as well as the strong exchange interactions of Fe-Co and Fe-Ni pairs. Experimental results corroborate these findings, indicating the appropriate addition of Co and minor addition of Ni can significantly enhance the total magnetic moment of the alloy. Overall, this research provides critical insights for optimizing Fe-based amorphous alloys and paves the way for developing high-performance magnetic materials.

References

[1] Li H X, Lu Z C, Wang S L, Wu Y, Lu Z P 2019 Prog. Mater. Sci. 103 235

[2] Silveyra J M, Ferrara E, Huber D L, Monson T C 2018 Science 362 eaao0195

[3] Wang W H, Dong C, Shek C H 2004 Mater. Sci. Eng. R 44 45

[4] Seghairi N, Bendjemil B, Lavorato G, Castellero A, Baricco M 2012 Chin. Phys. Lett. 29 118102

[5] Huo J, Li K, Zang B, Gao M, Wang L M, Sun B, Li M, Song L, Wang J Q, Wang W H 2022 Chin. Phys. Lett. 39 046401

[6] Ohta M, Hasegawa R 2017 IEEE Trans. Magn. 53 2000205

[7] Kasai S, Namikawa M, Hiratani T 2016 JFE Tech. Rep. 14
[8] Shi L, Yao K 2020 Mater. Des. 189 108511
[9] Ri M C, Ding D W, Sun B A, Wang J Q, Zhu X S, Wang B B, Wang T L, Qiu Q Q, Huo L S, Wang W H 2018 J. Non·Cryst. Solids 495 54
[10] Qi Z G, Chen Q, Wang Z X, Song Z Q, Kim K B, Pang J, Zhang X H, Wang W M 2024 NPJ Mater. Degrad. 8 28
[11] Duan X Y, Ju S W, Li Y H, Zhu Z W, Zhang H F, Zhang W 2023 J. Non·Cryst. Solids 616 122480
[12] Qi X J, You J H, Zhou J F, Qiu K Q, Cui X L, Tian J, Li B L 2023 Phys. Status Solidi A 220
[13] Shi L, Hu X, Li Y, Yuan G, Yao K 2021 Intermetallics 131 107116
[14] Xiao J H, Ding D W, Li L, Sun Y T, Li M Z, Wang W H 2024 Chin. Phys. B 33 076101
[15] Hou L, Fan X, Wang Q, Yang W, Shen B 2019 J. Mater. Sci. Technol. 35 1655
[16] Li X, Zhou J, Shen L, Sun B, Bai H, Wang W 2023 Adv. Mater. 35 2205863
[17] Wang F, Inoue A, Han Y, Zhu S L, Kong F L, Zanaeva E, Liu G D, Shalaan E, Al-Marzouki F, Obaid A 2017 J. Alloys Compd. 723 376
[18] Yang W, Liu H, Zhao Y, Inoue A, Jiang K, Huo J, Ling H, Li Q, Shen B 2014 Sci. Rep. 4 6233
[19] Chen P B, Liu T, Kong F Y, Wang A D, Yu C Y, Wang G, Chang C T, Wang X M 2018 J. Mater. Sci. Technol. 34 793
[20] Yu Q, Wang X D, Lou H B, Cao Q P, Jiang J Z 2016 Acta Mater. 102 116
[21] Ding J, Ma E, Asta M, Ritchie R O 2015 Sci. Rep. 5 17429
[22] Yuan C C, Deng C, Zhang H P, Li M Z, Shen B L 2019 Interetallics 112 106501
[23] Ma H J, Shen K C, Pan S P, Zhao J, Qin J Y, Kim K B, Wang W M 2015 *J. Non·Cryst. Solids* 425 67
[24] Huang Z, Zhang Y, Shi R, Fu P, Zhu W, Tao P, Dong H, Yang Y 2024 Mater. Today Commun. 39 108604
[25] O'Handley R C, Boudreaux D S 1978 Phys. Status Solidi A 45 607
[26] Tong X, Zhang Y E, Shang B S, Zhang H P, Li Z, Zhang Y, Wang G, Liu Y H, Zhao Y, Zhang B, Ke H B, Zhou J, Bai H Y, Wang W H 2024 Nat. Mater. 23
[27] Kresse G, Joubert D 1999 Phys. Rev. B 59 1758
[28] Blochl P E 1994 Phys. Rev. B 50 17953
[29] Faber T E, Ziman J M 1965 Philos. Mag. 11 153
[30] Ma S, Ran Y, Liang X, Jiang L, Li Y, Wang X, Yao M, Zhang W 2022 J. Alloys Compd. 902 163637
[31] Jiang J, Li Q, Duan H, Li H 2017 Comput. Mater. Sci. 130 76
[32] Wang Y C, Zhang Y, Makino A, Liang Y Y, Kawazoe Y 2014 IEEE Trans. Magn. 50 2003704
[33] Finney J L 1977 Nature 266 309
[34] Honeycutt J D, Andersen H C 1987 J. Phys. Chem. 91 4950